EUROPEAN **S**YNCHROTRON **R**ADIATION **F**ACILITY

INSTALLATION EUROPEENNE DE RAYONNEMENT
SYNCHROTRON

ESRF

Experiment Report Form

The double page inside this form is to be filled in by all users or groups of users who have had access to beam time for measurements at the ESRF.

Once completed, the report should be submitted electronically to the User Office using the **Electronic Report Submission Application:**

http://193.49.43.2:8080/smis/servlet/UserUtils?start

Reports supporting requests for additional beam time

Reports can now be submitted independently of new proposals – it is necessary simply to indicate the number of the report(s) supporting a new proposal on the proposal form.

The Review Committees reserve the right to reject new proposals from groups who have not reported on the use of beam time allocated previously.

Reports on experiments relating to long term projects

Proposers awarded beam time for a long term project are required to submit an interim report at the end of each year, irrespective of the number of shifts of beam time they have used.

Published papers

All users must give proper credit to ESRF staff members and proper mention to ESRF facilities which were essential for the results described in any ensuing publication. Further, they are obliged to send to the Joint ESRF/ ILL library the complete reference and the abstract of all papers appearing in print, and resulting from the use of the ESRF.

Should you wish to make more general comments on the experiment, please note them on the User Evaluation Form, and send both the Report and the Evaluation Form to the User Office.

Deadlines for submission of Experimental Reports

- 1st March for experiments carried out up until June of the previous year;
- 1st September for experiments carried out up until January of the same year.

Instructions for preparing your Report

- fill in a separate form for each project or series of measurements.
- type your report, in English.
- include the reference number of the proposal to which the report refers.
- make sure that the text, tables and figures fit into the space available.
- if your work is published or is in press, you may prefer to paste in the abstract, and add full reference details. If the abstract is in a language other than English, please include an English translation.

ESRF	**Experiment title:** High energy angle resolved photoemission	**Experiment number**: HE-1009
Beamline: ID08	**Date of experiment**: from: 2000 to: 2003	**Date of report**: 2003-09-10
Shifts:	**Local contact(s)**: Nicholas Brookes, Celine De Nadai	*Received at ESRF:*

Names and affiliations of applicants (* indicates experimentalists):

Oscar Tjernberg, Martin Månsson, Thomas Claesson,
Claudia Dallera, Marco Finazzi, Lamberto Duo,
Hao Tjeng, Christian Schüssler-Langeheine, Thomas Koethe, Csiszar Szilard
Sarnjeet Dhesi, Alberto Tagliaferri
Marco Grioni, Joel Mesot
Celine De Nadai, Federica Venturini and Nicholas Brookes

Report:

Background

The long term project on high energy angle resolved photoemission (HARPES) that was approved by the beam time review committee in 2000 was the continuation of in-house work that was conducted at ID12B from the fall of 1997 and onwards. The aim of the project was to develop an experimental setup capable of performing angle resolved photoemission spectroscopy in the 400-1000 eV range with sufficient angular and energy resolution to study valence band dispersion. This requires very high photon flux because of the low cross-sections, angular resolution on the order of 0.1^{o} and an energy resolution on the order of 100 meV. The main interests for going to high photon energies are increased bulk sensitivity, a free electron like photoelectron decoupled from the rest of the system and an approximately linear relation between electron momentum and emission angle. These properties make HARPES an excellent experimental tool in the study of strongly correlated 3D system as well as systems were the surface electronic structure is expected to differ from the bulk.

Technical status

The technical part of this project consisted of the construction and installation of a new beam line endstation built around a Gammadata SES-2002 electron energy analyzer. The energy range and angular resolution put new requirements on the experimental setup and in particular on the analyzer and the sample alignment. Even though there are still technical improvements to be made, as discussed below, the project has successfully achieved the technical goals. At present, the system is capable of recording valence band spectra with an angular resolution of 0.15^{o} in the analyzer slit direction and 0.2^{o} perpendicular to the slit. An early problem with defects on the analyzer entrance slits has been resolved by exchanging the slits. These repairs were done during the spring 2002 and resulted in a 6 month delay of the project. The combined energy resolution obtainable with the system is of course related to the recording time and cross-section but for most samples,

spectra with 100-150 meV resolution can be recorded in approximately 1h with photon energies in the 400-800 eV range.

The requirements on sample alignment lead to the construction of a sample holder with six degrees of freedom. The need for having a vertical tilt angle motion has to some extent been decreased by positioning the analyzer entrance slit in the vertical plane. This has as a consequence that an offset in the tilt angle of the sample only shifts the angular window of the analyzer and is therefore not something that needs to be corrected in most cases. The other angular motions are, however, still critical and improvements in the calibration and precision in these movements would facilitate the experimental work.

The technical status of setup is summarized in the following list:

- Analyzer with 0.15 ^{o} / 100meV resolution. (The energy resolution is flux limited.)
- Measurement chamber with $<10^{-10}$ mbar, LEED equipped
- Sample holder with six degrees of freedom and 23 K on sample
- Preparation chamber witch $<10^{-9}$ mbar, heating, sputtering and evaporation
- Fast entry load-lock and sample storage
- Software for automatic data acquisition permitting multiple scans for varying energies and polar angles.

Possible technical improvements

Part of the sample alignment is at present a tedious process since azimuthal angles and centering of the manipulation rotational axes has to be done in a trial and error fashion. Technical solutions to facilitate this process has been discussed with the beam line staff and are to some extent envision for the future.

It has also become clear that many samples do not fulfill the very high flatness requirements that are posed by high energy measurements. This problem is related to spot size since a smaller spot size would increase the chance of finding a sufficiently flat part of the sample surface. In general terms the signal to noise ratio therefore scales with the spot size. It would thus be very beneficial for angular resolved measurement if the x-ray beam could be refocused horizontally as well as vertically.

The linearity of the angular distribution and resolution of the analyzer is a trade off with the spot size. The relatively small spot size at ID08 permits a better than standard angular distribution and linearity. The Gammadata company has been contacted in this matter and have promised to deliver new analyzer voltage tables that would exploit this. So far these tables have not been delivered.

A new detector read out system will soon be available on the market. This new system will permit point by point calibration of the detection system and should therefore drastically increase the possibility of doing experiments that rely on relative intensity differences.

Highlights of experimental results

During the first two runs of the project, the major part of the beam time was spent on verifying the feasibility of high energy ARPES and the influence of temperature and photon energy on phonon scattering in the photoemission process. The valence band dispersions of Al, Cu, $TaSe_2$ and NiO were measured during these runs and some of the results are shown below.

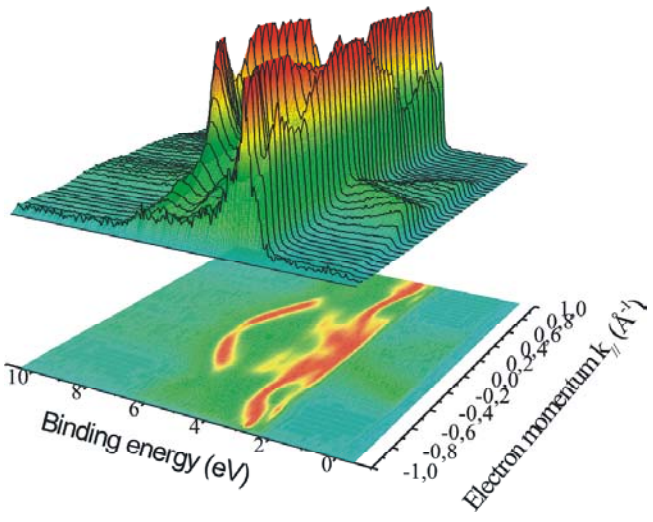

In the figure on the left, Cu valence band data measured at a photon energy of 580 eV are presented. Due to the analyzer slit problems mentioned above, the relative intensities are not correct and the spectrum has been normalized to equal maximum intensity. Irrespective of this, the Cu d band dispersion can be clearly seen between 2 and 8 eV binding energy as can the Cu s-p band with its parabolic dispersion crossing the Fermi level at a parallel momentum of approximately 0.4 $Å^{-1}$.

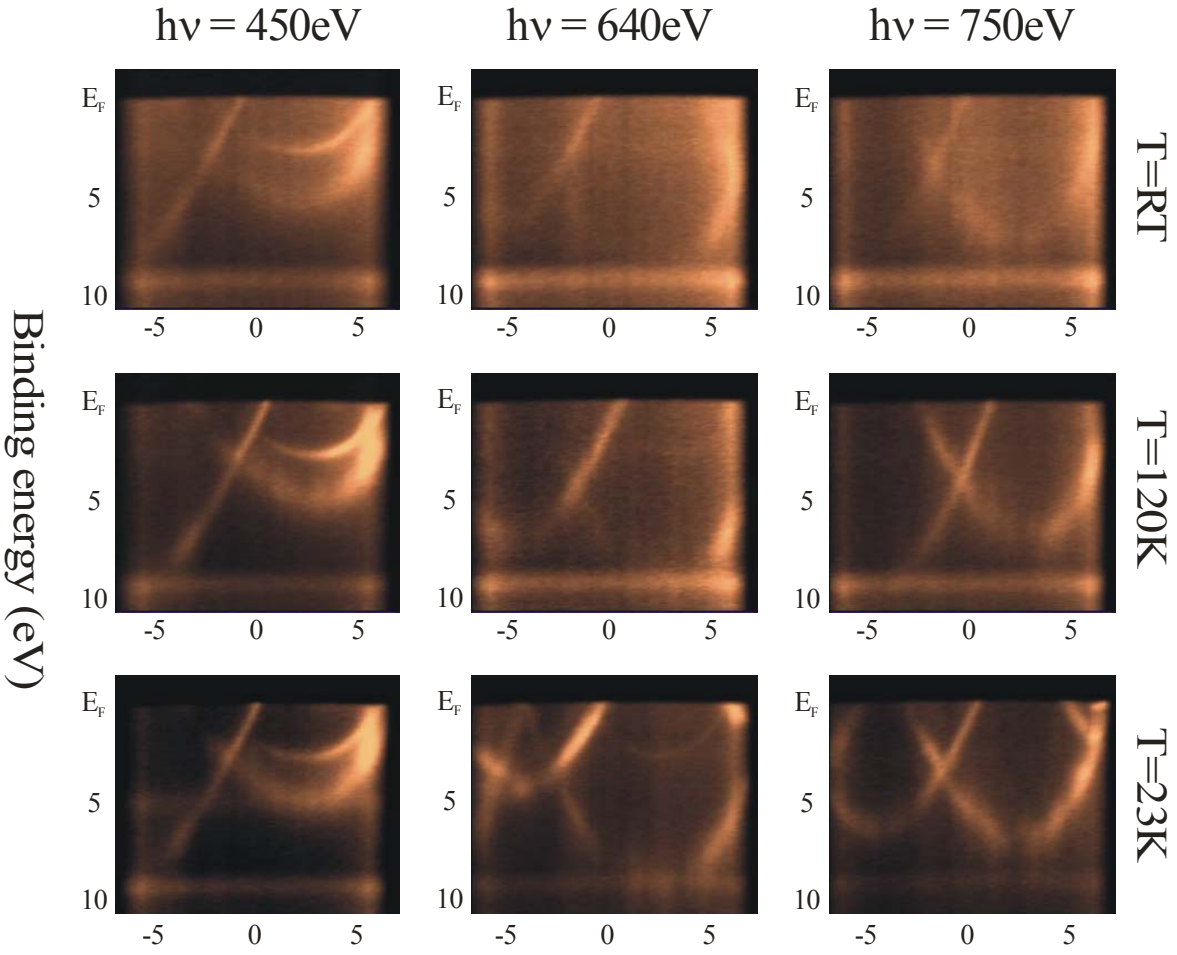

In the figure above, Al valence band data for three different temperatures and photon energies are presented. Both the parabolic in plane dispersion as well as dispersion in the normal direction as a function of photon energy are clearly seen. Another prominent feature in these data is the temperature dependence of the signal to background ratio. The result of a more detailed study of the momentum broadening as a function of photon energy and temperature is shown in the figure on the left. It demonstrates that the peak width in momentum increases with increasing photon energy as expected. Unexpected is, on the other hand, that the peak width for the lower temperatures decreases in going from 640 eV to 760. This is difficult to explain and might be due to something that is not intrinsic to the photoemission process. It is noteworthy that the smallest MDC width at 760 eV is approximately 0.15 $Å^{-1}$. This value should be compared to the photon momentum of 0.19 $Å^{-1}$, which demonstrates that the photon momentum does not contribute substantially to the broadening but rather induces a shift ot the measured dispersion.

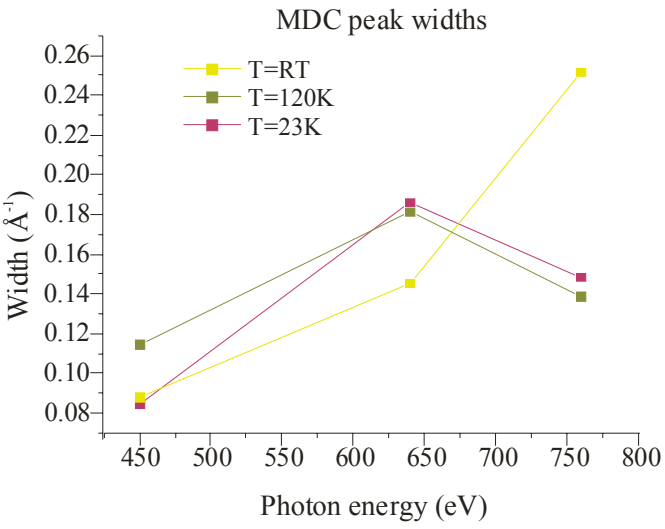

As an example of the direct application of the HARPES technique to a strongly correlated three-dimensional material, we have measured the prototypical Mott-Hubbard system NiO. A color topological plot of the NiO valence band, recorded with hν=610 eV, is shown below. Blue color indicates low intensity and green, yellow and red indicate increasingly higher intensities. (Note that the color scale is non-linear.) A very high intensity is seen in the 2-4 eV region. This intensity is according to calculations due to Ni $t2_g$ bands[i]. At 9-10 eV binding energy there is a feature that disperses to lower binding energy and back as one goes from Γ to X. This feature is most likely Ni e_g related. Apart from these features, there is also a highly dispersive feature that crosses over from the upper to the lower part of the valence band as the momentum increases. The interesting point here is that the main intensity seems to follow the dashed line in the figure while the

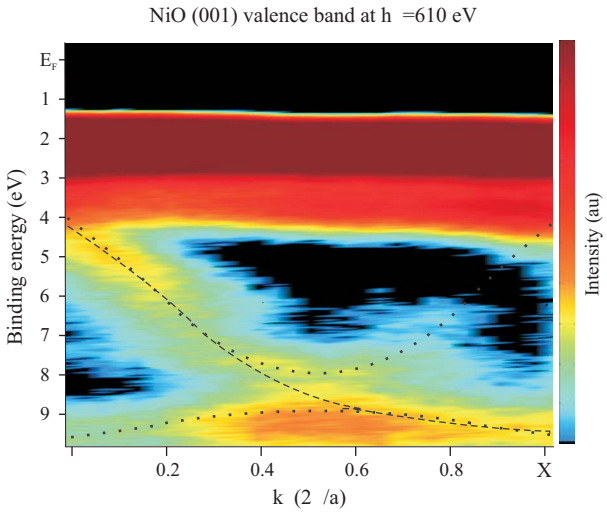

dispersion follows the dotted lines. This kind of behavior has not been observed before in NiO and indicates the presence of two competing potential of different periodicity. The main intensity follows the dispersion resulting from the normal lattice potential whereas the symmetric dispersion is the result of the antiferromagnetic ordering with twice the periodicity. It has been shown[ii] that the amount of spectral weight transferred into the bands originating from the competing potential scales with the strength of the potential. The relative weight in the feature that disperses towards lower binding energy for $k > 0.5$ can therefore be used to extract an estimate for the strength of the antiferromagnetic potential. Note also that the spectral intensity in the 9 eV feature is distinctively higher at X as compared to Γ. Low energy ARPES data display additional peaks in the 5 eV region and they have been interpreted as proof of antiferromagnetic influence on the band structure[iii,iv]. The data presented here do, on the other hand, not show any sign of an extra flat band in this region. In our opinion, the difference between our high-energy data and the low energy data stems from the assumption of a free electron like final state in the analysis of the low energy data. This assumption is highly questionable in a strongly correlated system such as NiO and is therefore likely to introduce erroneous features in the experimentally derived dispersion relations. Further details and discussions about these results can be found in the appended preprint.

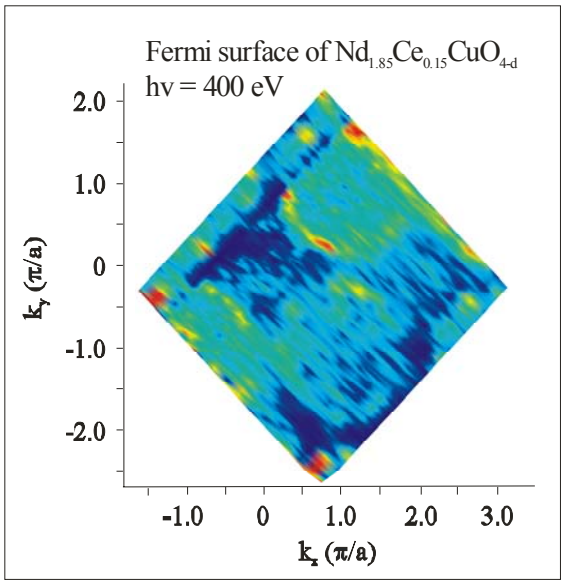

Another topic that has been studied within the project is the photon energy dependence of angle resolved photoemission data from the high temperature superconductors. Unfortunately, despite the use of many different samples, the above mentioned problem with highly flat surfaces limited our results to the $Nd_{2-x}Ce_xCuO_{4-\delta}$ (NCCO) system. By performing angular scans covering the whole Brillouin zone, we were able to reconstruct the experimental Fermi surface for NCCO. The result of such a compilation is shown to the left. The very low intensity at the Fermi level in these materials makes these kinds of measurements at high energy very difficult. From the figure it is, however, clear that there are repeated Fermi hole like surfaces centered around (π,π). The nature of the Fermi surfaces in cuprates has been a source of debate in recent years because of their apparent photon energy dependence. Our results confirm the hole like nature of the Fermi surface in NCCO and rules out any remaining doubt in this issue. By utilizing the required symmetry of the Fermi surface and averaging over the repeated surfaces in the figure it is possible to produce a Fermi surface image of higher quality. The result of such a folding and averaging is shown on the left. The shape and intensity around the Fermi surface is now well defined. The almost diamond like shape of the Fermi surface is much more quadratic than the rounder shape observed at low energy[v]. A possible explanation for this difference is the increased bulk sensitivity in our measurements. In this scenario, the bulk electronic structure would differ from the surface due to the difference in interlayer coupling. The question about doping differences between the surface and bulk also arises in this context. By measuring the Fermi surface volume we determine the doping level to x=0.16 which is close to the nominal doping of x=0.15 and thus in agreement with Luttinger's

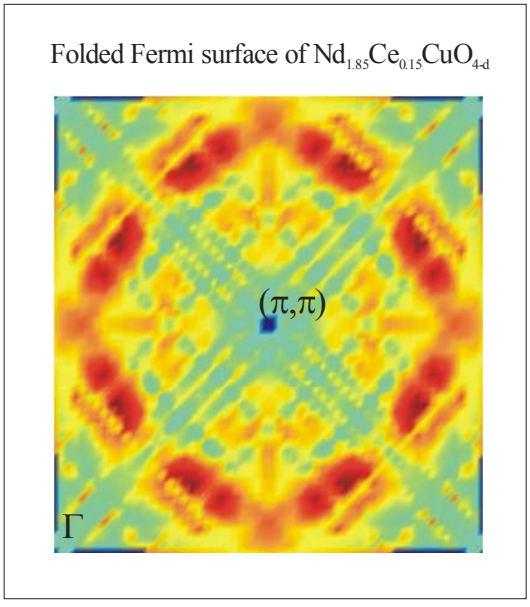

theorem. This fact implies that the bulk electronic structure fulfills the conditions for Luttinger's theorem to be valid. Earlier low energy data confirms that also the surface doping is in agreement with Luttinger's theorem. It would thus seem that the difference in shape between the Fermi surfaces measured at low and high photon energy is not due to differences in doping but rather in environment. The uncertainties in the determination of the Fermi surface volume are, however, so large that it is not possible to completely rule out differences in doping between the bulk and the surface. Apart from differences in the shape of the Fermi surface between the low and high energy data there is also a difference in intensity. Where the intensity is high in our data (dark red in the figure above) the low energy data show low intensity. The low intensity in the low energy data was attributed to π,π scattering that connects the Fermi surfaces in neighboring zones and thus decreases the quasiparticle lifetimes at the Fermi level. By comparing data recorded at 16.5eV, 55eV and our data it seems clear that there is no sign of significant π,π scattering and the low intensity spots in the 16.5 eV data were most likely due to matrix element effects. More details on these issues and further experimental data are presented in the appended manuscript below.

Finally, we have very recently attempted obtain photoelectron interference patterns. The analysis of these data is currently under way but an example of an observed pattern is shown below.

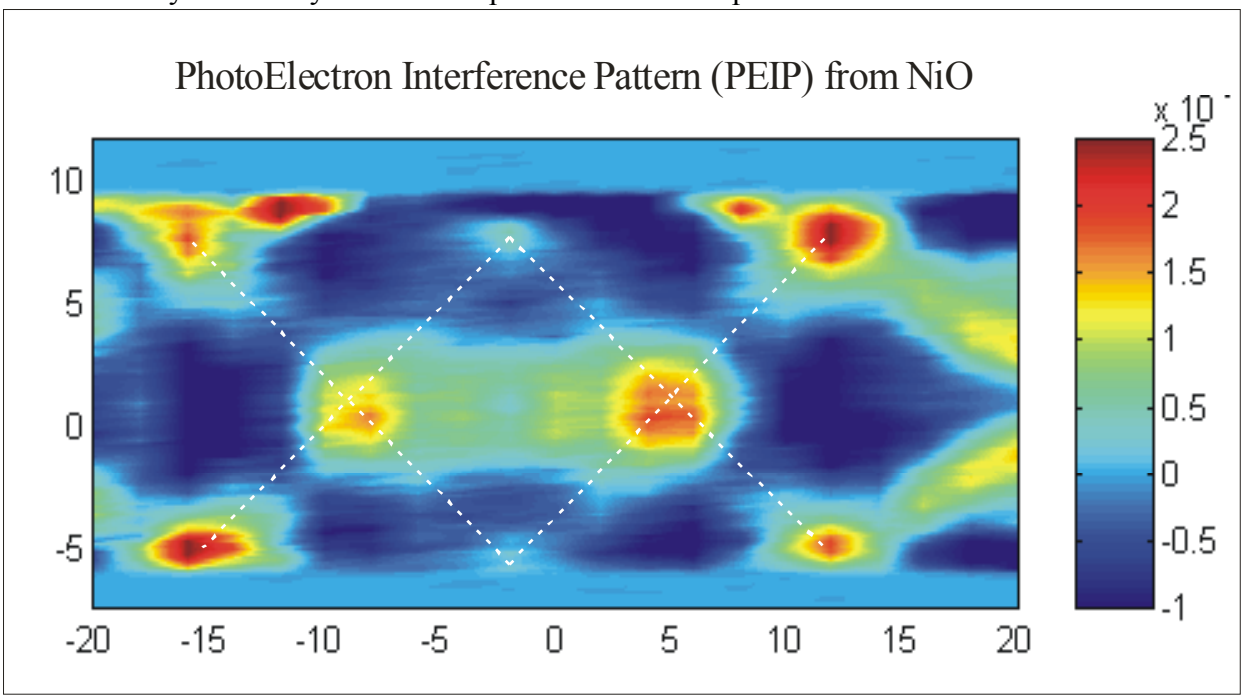

The intensity pattern as a function of angle has been obtained by integrating the *d* band intensity from a NiO thin film measured with the photon energy tuned to the Ni 2p resonance at hν = 852 eV. Even though the nonlinear properties of the analyzer make the data analysis difficult one can clearly see a diamond like pattern. (White dashed lines are guides to the eye.) The angles between the observed spots correspond approximately to the angles one would expect for a pattern that results from interference between electrons coherently emitted from different Ni atoms. Further analysis of the data as well as comparisons with multiple scattering photoelectron diffraction calculations are necessary to determine if the observed pattern can be explained within photoelectron diffraction theory or whether the pattern is the result of interference between coherently emitted multiple electrons.

---

[i] O. Bengone et al. Phys. Rev. B **62**, 16392 (2000)
[ii] J. Voit et al. Science **290**, 501 (2000)
[iii] Z.-X. Shen et al. Phys. Rev. Lett. **64**, 2442 (1990), Phys. Rev. B **42**, 1817 (1990), *ibid*. **44**, 3604 (1991)
[iv] H. Kuhlenbeck et al. Phys. Rev. B 43, 1969 (1991)
[v] N.P. Armitage et al. Phys. Rev. Lett. **87**, 147003 (2001)

High energy angle resolved photoemission from NiO

O. Tjernberg, T. Claesson, and M. Månsson
*Laboratory of Materials and Semiconductor Physics, Royal Institute of Technology, Electrum 229, S-164 40 Kista, Sweden**

C. Dallera and M. Finazzi
INFM-Dipartimento di Fisica, Politecnico di Milano, Piazza Leonardo da Vinci 32, I-20133 Milano, Italy

C. De Nadai, F. Venturini, and N.B. Brookes
ESRF-European Synchrotron Radiation Facility, BP 220, 38043 Grenoble, France
(Dated: May 22, 2003)

High-energy angle resolved photoemission has been applied to the prototypical strongly correlated system NiO. Valence band spectra recorded at a photon energy of 610 eV are presented and the results show that the extension of angle resolved photoemission to the high energy range is important for this kind of system. The observed valence band dispersion show signs of the Brillouin zone halving that accompanies the antiferromagnetic ordering and can therefore be taken as evidence for the influence of the magnetic ordering on the electronic structure.

PACS numbers: Valid PACS appear here

NiO is often considered as the prototypical strongly correlated system and was taken as an example already in N.F. Mott's seminal 1949 paper[1]. It has been extensively studied[2] for many years but a satisfactory understanding of its electronic structure is still lacking. The most obvious problem in the description of NiO is that it has a partially empty d-band but is, nonetheless, an insulator with a large band gap on the order of 4 eV. Correspondingly, local density approximation (LDA) calculations describes NiO as a metal rather than an insulator. A straightforward remedy to this problem is to include the magnetic ordering in the calculations and to perform local spin density approximation (LSDA) calculations. Such a calculation correctly describes NiO as an insulator albeit with a small band gap. The possible importance of magnetism in explaining the insulating behavior of NiO was pointed out almost two decades ago[3, 4]. Even though the LSDA approach probably underestimates the importance of strong correlation in the Ni $3d$ band it raises the important question of the relation between antiferromagnetic order in NiO and the valence band electronic structure. A very powerful technique in the investigation of electronic structure is angle resolved photoemission (ARPES). One of the strongest arguments for the use of ARPES is the ability to directly measure the spectral function $A(\omega, k)$. This argument is unfortunately not really true because of matrix element effects as well as the problem of determining the k vector component perpendicular to the sample surface. In recent years, there has been impressive progress in the energy as well as angular resolution obtainable with ARPES[5] and high resolution ARPES has been extensively applied to high T_c superconductors and related two-dimensional materials. Unfortunately, the progress has not been extended to three-dimensional strongly correlated compounds. The inability to apply ARPES to these materials in a straightforward way is a serious impairment that stems from the non-conservation of electron momentum in the direction perpendicular to the sample surface. In one or two-dimensional materials this is not a serious problem since no dispersion is expected in this direction. For three-dimensional materials on the other hand, the dispersion in the perpendicular direction is as important as in any other direction and cannot be neglected. The classical way to deal with this problem has been to measure normal emission spectra as a function of excitation energy and to assume a free electron like final state. The assumption of a free electron like final state is obviously not a very good one for a strongly correlated compound if the excitation energy is low.

In this letter we present another approach to this problem and show that by going to high excitation energies and utilizing the latest advances in synchrotron radiation and electron detection techniques the energy versus momentum dispersion of the prototype system NiO can be determined in a straight forward manner. Furthermore, it is shown that earlier results indicating the influence of antiferromagnetic order on the dispersion relations were the result of difficulties with the application of low energy ARPES to this system. The high energy results presented here do, on the other hand, show a previously unobserved dispersion symmetry originating from the antiferromagnetic ordering.

In Fig.1, the photoelectron momentum and angles involved in an ARPES measurement at two different energies are depicted. In the low energy case, which is representative for typical UPS synchrotron or He lamp measurements, the kinetic energy of the photoelectron is ≈20

*Electronic address: oscar@kth.se

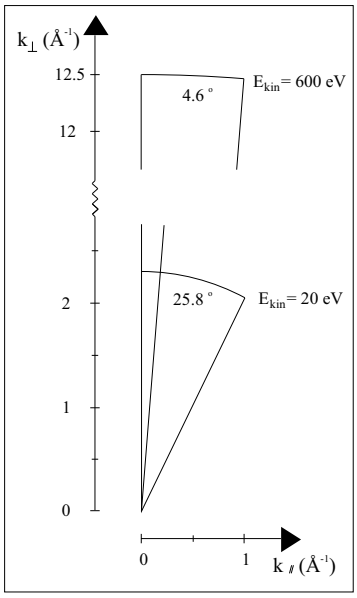

FIG. 1: A comparison of the electron momenta and angles involved in low and high energy angle resolved photoemission.

eV. As seen in Fig.1, the angle to cover a typical Brillouin zone is several tens of degrees and the corresponding k-space line is considerably curved. On the other hand, if the energy is increased to ≈600 eV, the angle needed to cover a Brillouin zone is on the order of a few degrees and the corresponding k-space curvature is small compared to the zone size. This fact implies that if parallel detection is used, the dispersion along a high symmetry line can be recorded in a single measurement even for a sample with a three dimensional electronic structure.

The high excitation energy has several other important advantages as compared to the corresponding low energy measurement. One advantage that is very important in the case of strongly correlated systems is that the high energy of the photoelectron results in a state that is effectively decoupled from the many body state of the system and thus free electron like. This is not necessarily true in the case of low energy ARPES where strong final state effects can effectively hamper the interpretation of spectra as noted below. Another advantage, in the case of bulk properties, is that the increased mean free path of the photoelectron enhances the bulk sensitivity of the measurement as compared to low excitation energies. In the energy range 20 - 100 eV where most ARPES measurements are conducted, the escape depth is minimal and the observed intensity dominated by the outermost atomic layer. At 600 eV or higher kinetic energies, the intensity is dominated by emission from the second and deeper layers. For materials where the surface electronic structure is different from the bulk this is of course very important. An example of the importance of the difference between bulk and surface electronic structure in strongly correlated materials is given by studies on Ce compounds where this difference has been shown to be very significant[6]. The advantages of going to high energy in ARPES come at the cost of lower cross-sections and lower photon energy resolution. Recent advances in photon source and detector technologies can resolve this problem to a large extent and some angular resolved spectra at high energy have already been obtained[7]. It is expected that in the near future, new and existing beamlines at third generation light sources will be able to collect angle resolved spectra with 0.05 degree angular resolution and ≈30 meV energy resolution at 700 eV.

At the European Synchrotron Radiation Facility ESRF a new high flux beam line for photons in the 400-1500 eV range was recently commissioned. The beam line, ID08, produces $\approx 10^{13}$ photons/s/0.1%BW on sample with a resolving power of ≈ 10000 at 400 eV. Coupled to the new beam line is an experimental chamber equipped with a Gammadata SES-2002 electron energy analyzer. This set-up permits the collection of ARPES spectra with an angular resolution of 0.15° along the analyzer slit and 0.2° in the perpendicular direction.

Attempts to apply low energy ARPES to NiO have focused on fits of normal emission data to free electron like final states[8–13]. A key issue in these studies is the relation between the antiferromagnetic ordering and the electronic structure. The low energy ARPES results were interpreted as supporting LSDA calculations where the antiferromagnetic structure of NiO is taken into account. In Fig.2, the results of LDA and LSDA calculations are shown. The calculations were performed with the WIEN2k program[14] using a cubic lattice with $a = 4.19\mathring{A}$. The obtained results agree well with earlier calculations[9, 11, 15, 16]. The top part of Fig.2 shows the LDA calculation for $\Gamma \rightarrow X$ (left) and $L = \pi/a(111) \rightarrow L = \pi/a(311)$ (right), while the bottom part shows the LSDA calculation for the $\Gamma \rightarrow X$ direction. In the LSDA calculation, the amount of Ni $3d$ character in the calculated bands has been indicated by the use of varying marker size. Comparing the top and bottom parts of Fig.2, one sees that the main effect of including the antiferromagnetic ordering is to reduce the size of the Brillouin zone (BZ) and thus to fold in the bands from the $L = \pi/a(111) \rightarrow L = \pi/a(311)$ direction into the $\Gamma \rightarrow X$ direction. As a result of this folding, there is a flat band at ≈5.5 eV binding energy in the antiferromagnetic calculation. Low energy ARPES data that showed features at or close to this band were therefore interpreted as evidence for the influence of magnetic ordering on the electronic structure. As mentioned above, the assumption of a free electron like final state is, however, not a reasonable assumption for a strongly correlated system at low excitation energies. Furthermore, because of the k-space curvature depicted in Fig.1, angular scans cannot be utilized to measure along a given symmetry line. As can also be seen in Fig.1, the angular scan do, however, give a good approximation of a linear scan at high energy. In Fig.3, such an angular scan is presented. The data were collected at room temperature, which is well below the Néel temperature of NiO

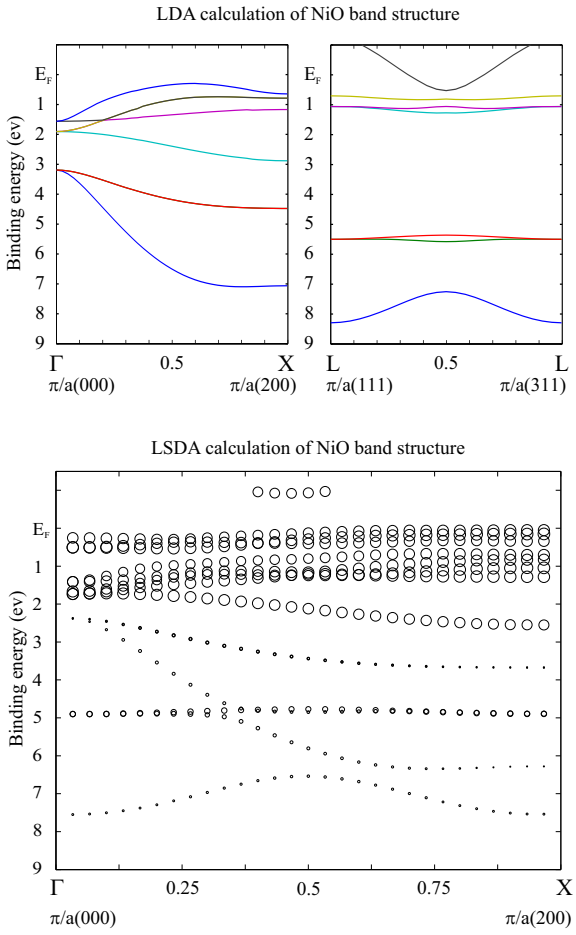

FIG. 2: Local density approximation calculations (top) and local spin density approximation calculations (bottom) for NiO. The marker size in the bottom figure indicates the amount of Ni $3d$ weight.

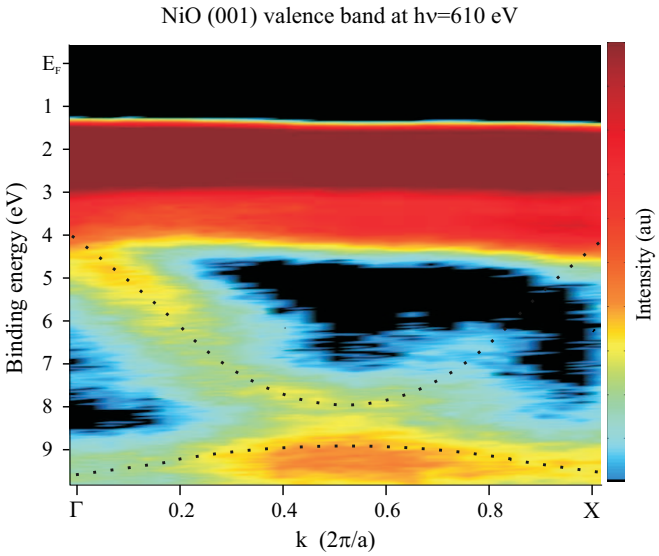

FIG. 3: Angle resolved photoemission data on the NiO valence band. The color scale is nonlinear in order to enhance low intensity features. The dotted black lines are guides to the eye.

($T_N = 525$K). The photon energy of 610 eV was chosen so that normal emission corresponds to the Γ-point. In order to enhance low intensity features, the color scale is nonlinear. At 2 eV binding energy, one sees the almost dispersionless high intensity Ni $3d$ bands. The Ni $3d$ labeling should, however, not be taken literally since these states are best described in a configuration interaction cluster model with strong O $2p$ Ni $3d$ hybridization. It has also been shown that the top of the valence band is of $3d^8\underline{L}$ character[17]($\underline{L}$ denotes a hole on the oxygen ligands) and that NiO therefore is a charge-transfer insulator[18]. Another weakly dispersing feature is observed at ≈ 9 eV binding energy but this feature is much less intense. The 9 eV band is reproduced by the LSDA calculation in the lower part of Fig.2 but has also been attributed to a Ni $3d^7$ satellite[19]. Between these two flat bands there is a weak but rapidly dispersing feature. The latter has also been observed by low energy ARPES and attributed to O $2p$ states because of its similarity to the calculated bands of O $2p$ character in Fig.2[9, 11, 15]. The low cross-section for this state seems to support this[20]. There is, on the other hand, no sign of any flat band in the 5 to 7 eV binding energy region as predicted by the LSDA and LSDA+U calculations and reported in the low energy ARPES measurements. As seen from Fig.2, the amount of Ni $3d$ character in the flat band is expected to be higher than in the rapidly dispersing band and the cross-section for the flat band should therefore be correspondingly higher. The fact that no flat band is observed in our measurements is therefore evidence that the observation of such a band in low energy ARPES[8–11] was most likely due to non-free-electron like final states. One should, however, not forget that the LSDA calculation describes the ground state of the system whereas the photoemission final state is an excited state and that a disagreement between the two not necessarily invalidates the LSDA approximation. It is, nevertheless, clear from the present data that LSDA and LSDA+U calculations cannot be used to describe the observed valence band dispersion. The current experimental results do, however, confirm that there are rapidly dispersing features and that any theoretical description of NiO needs to take the translational symmetry into account. A more important result that is seen in Fig.3 is that the dispersion seems to be symmetric around the $k = 0.5$ (in units of $2\pi/a$) point. This is seen both through the beginning of a feature dispersing up again from high to low binding energy as k is increased from ≈ 0.5 to X as well as in the weak dispersion in the 9 eV band. This symmetry has not been observed previously and is not expected unless the halving of the Brillouin zone size due to the antiferromagnetic ordering is taken into account. As seen in Fig.2 and mentioned above, the main effect of the inclusion of magnetic ordering is to fold in the bands from $(\pi/a)(111)$ to $(\pi/a)(311)$. Since this is a consequence of

the Brillouin zone size reduction resulting from the antiferromagnetic ordering, it does not depend on the exact form of the bands and a similar result with symmetric bands can be expected even if these bands might have a dispersion quite different from what is seen in Fig.2. As a consequence, the dispersion symmetry observed in Fig.3 is evidence of the Brillouin zone size reduction resulting from the antiferromagnetic ordering. The exact shape of the dispersion is, on the other hand, not in agreement with the LSDA calculation and adds further to the discrepancy between the calculation and the observed dispersion. Even though the dispersion in Fig.3 is symmetric around the $k = 0.5$ point, the intensity is not. It is seen that the 9 eV band carries more spectral weight in the $k = 0.5 \rightarrow 1$ region whereas the rapidly dispersing O band carries more weight in the $k = 0 \rightarrow 0.5$ region. This fact is easily explained by the continuous transfer of spectral weight that occurs when the periodicity of the lattice is changed by the introduction of a new potential. The spectral weight in the bands introduced by the new symmetry increases smoothly as the strength of the potential is increased[21]. In the present case, this implies that spectral weight in the rapidly dispersing band below $k = 0.5$ should be transferred to the new branch of this band that has appeared above $k = 0.5$. Similarly, one expects weight in the 9 eV band to be transferred from the right to the left. The extent to which this occurs is a measure of the relative strength of the antiferromagnetic potential as compared to the non-magnetic lattice potential. As seen from Fig.3, the main intensity is still confined to what can be called the non-magnetic band but there is also a non negligible intensity in the rapidly dispersing band above $k = 0.5$. This shows that the antiferromagnetic potential is a weak but non negligible perturbation on the non-magnetic lattice potential. While contradicting previous results interpreted as antiferromagnetic influence on the valence band dispersion, the present data therefore show a new and more direct form of evidence of antiferromagnetic influence on the valence band.

In conclusion, the presented data show the feasibility of high energy angle resolved photoemission and that this kind of measurements can provide new and valuable information about strongly correlated three-dimensional systems. In the present example of measurements on NiO, the observed dispersion was not in complete agreement with earlier low energy measurements. While indications of a flat band around 5 eV binding energy in low energy measurements was not observed in the present data, a previously not observed symmetry in the dispersion gives direct evidence for the importance of the antiferromagnetic potential on the valence band electronic structure. It is expected that many new results will emerge from the application of high energy angle resolved photoemission to other strongly correlated three-dimensional materials as well as materials with differences between bulk and surface electronic structure. Most transition metal and rare earth compounds have p and d levels in the 500-1000 eV range, which also opens up the possibility of doing selective resonant angle resolved photoemission on a wide range of materials.

Valuable discussions and comments from L.H. Tjeng, M. Grioni and U.O. Karlsson are gratefully acknowledged as is the technical support from K. Larsson. This work was in part supported by the Swedish Research Council, the Swedish Foundation for Strategic Research and the Göran Gustafsson Foundation.

[1] N. F. Mott, Proc. Phys. Soc. London Sect. A **62**, 416 (1949).
[2] S. Hüfner, Adv. in Phys. **43**, 183 (1994), and references therein.
[3] K. Terakura, A. R. Williams, T. Oguchi, and J. Kübler, Phys. Rev. Lett. **52**, 1830 (1984).
[4] K. Terakura, T. Oguchi, A. R. Williams, and J. Kübler, Phys. Rev. B **300**, 4734 (1984).
[5] Y. Baer, M. G. Garnier, D. Purdie, P. Segovia, and M. Hengsberger, J. Electron Spectrosc. Relat. Phenom. **114-116**, 257 (2001).
[6] L. Duo, Surface Science Reports **32**, 233 (1998).
[7] S. Suga and A. Sekiyama, J. Electron Spectrosc. Relat. Phenom. **124**, 81 (2002).
[8] Z.-X. Shen, C. K. Shih, O. Jepsen, I. Lindau, W. E. Spicer, and J. W. Allen, Phys. Rev. Lett. **64**, 2442 (1990).
[9] Z.-X. Shen, R. S. List, D. S. Dessau, B. O. Wells, O. Jepsen, A. J. Arko, R. Barttlet, C. K. Shih, F. Parmigiani, J. C. Huang, et al., Phys. Rev. B **44**, 3604 (1991).
[10] H. Kuhlenbeck, G. Odorfer, R. Jaeger, G. Illing, M. Menges, T. Mull, H.-J. Freund, M. Pohlchen, V. Staemmler, S. Witzel, et al., Phys. Rev. B **43**, 1969 (1991).
[11] O. Tjernberg, S. Söderholm, T. Rogelet, U. O. Karlsson, M. Qvarford, I. Lindau, C.-O. Almbladh, and L. J. Hellbom, Vacuum **46**, 1215 (1995).
[12] Z.-X. Shen, P. A. P. Lindberg, C. K. Shih, W. E. Spicer, and I. Lindau, Physica C **162-164**, 1311 (1989).
[13] Z.-X. Shen, R. S. List, D. S. Dessau, A. J. Arko, R. Barttlet, O. Jepsen, B. O. Wells, and F. Parmigiani, Solid State Comm. **79**, 623 (1991).
[14] P. Blaha, K. Schwarz, G. K. H. Madsen, D. Kvasnicka, and J. Luitz, *An Augmented Plane Wave + Local Orbitals Program for Calculating Crystal Properties* (Karlheinz Schwarz, Techn. Universität at Wien, Austria, 2001).
[15] O. Bengone, M. Alouani, P. Blochl, and J. Hugel, Physical Review B (Condensed Matter) **62**, 16392 (2000).
[16] S. Massidda, A. Continenza, M. Posternak, and A. Baldereschi, Phys. Rev. B **55**, 13494 (1997).
[17] O. Tjernberg, S. Söderholm, U. O. Karlsson, G. Chiaia, M. Qvarford, H. Nylén, and I. Lindau, Phys. Rev. B **53**, 10372 (1996).
[18] J. Zaanen, G. A. Sawatzky, and J. W. Allen, Phys. Rev. Lett. **55**, 418 (1985).

[19] G. A. Sawatzky and J. W. Allen, Phys. Rev. Lett. **53**, 2339 (1984).
[20] J. J. Yeh and I. Lindau, Atom. data and nucl. data tables **32**, 1 (1985).
[21] J. Voit, L. Perfetti, F. Zwick, H. Berger, G. Margaritondo, G. Grüner, H. Höchst, and M. Grioni, Science **290**, 501 (2000).

Angle resolved photoemission from $Nd_{1.85}Ce_{0.15}CuO_4$ using high energy photons: a Fermi surface investigation

T. Claesson,[1,*] M. Månsson,[1] C. Dallera,[2] C. Schüssler-Langeheine,[3]
F. Venturini,[4] N.B. Brooks,[4] and O. Tjernberg[1]

[1] *Laboratory of Materials and Semiconductor Physics, Royal Institute of Technology, Electrum 229, S-164 40 Kista, Sweden*

[2] *INFM-Dipartimento di Fisica, Politecnico di Milano, Piazza Leonardo da Vinci 32, I-20133 Milano, Italy*

[3] *II. Physikalisches Institut der Universität zu Köln, Zülpicher Str. 77, D-50937 Köln, Germany*

[4] *ESRF-European Synchrotron Radiation Facility, BP 220, 38043 Grenoble, France*

(Dated: September 15, 2003)

Abstract

We have performed an angle resolved photoemission study on a single crystal of the optimally electron doped (n-type) cuprate superconductor $Nd_{2-x}Ce_xCuO_4$ ($x = 0.15$) at a photon energy of 400 eV. The Fermi surface is mapped out and is, in agreement with earlier measurements, of hole-type with the expected Luttinger volume. However, comparing with previous low energy measurements, we observe a different Fermi surface shape and a different distribution of spectral intensity around the Fermi surface contour.

PACS numbers: Valid PACS appear here

*Electronic address: tcl@kth.se

I. INTRODUCTION

Among the high-temperature cuprate superconductors only a small family can be doped with electrons (n-type), $Nd_{2-x}Ce_xCuO_4$ (NCCO) is one of them. The dominating amount of experimental work in this field has been devoted to the much larger family of hole-doped (p-type) materials and recent experiments have shown evidence for strongly contrasting behaviour between the two families [1]. The undoped parent compounds of both p- and n-type cuprate superconductors are antiferromengettic (AF) insulators [2]. An important aspect of cuprate high-T_c superconductivity is whether there exists a symmetry in the doping/temperature phase diagram when the AF parent is doped away from the insulating state with either electrons or holes. New studies of NCCO and the other n-type cuprates can give the information needed to resolve this issue.

Angle resolved photoemission spectroscopy (ARPES) is, because of its capability of directly measuring the spectral function $A(\omega, \vec{k})$, a very powerful technique in the study of the electronic structure of this class of materials. A number of recent ARPES studies of NCCO have shed new light on several central concepts of its electronic structure, for instance the symmetry of the superconducting gap [3], the doping dependence [4] and pseudogap-like effects [5].

The above-mentioned studies have been performed at relatively low photon energies (up to 55 eV), whereas the data we present here has been acquired at an excitation energy of 400 eV. High photon energy gives increased photoelectron mean free path and hence increased bulk sensitivity. Increasing the kinetic energy from around 16 eV to around 400 eV roughly doubles the photoelectron escape depth. The use of high photon energies also gives the possibility to investigate whether features seen in low energy data are real or could be caused by matrix-element effects.

Here we report a high photon energy ($h\nu = 400$ eV) angle resolved photoemission study of a $Nd_{2-x}Ce_xCuO_4$ ($x = 0.15$) single crystal at a temperature $T \approx 24K$. We observe a Fermi surface of hole-type with a volume respecting Luttinger's theorem [6], confirming previous measurements at lower photon energies [4, 5]. A detailed analysis of the Fermi surface reveals several features which deviate from the characteristics observed at lower photon energies [4, 5]. We see a different shape of the Fermi surface and a different variation of ARPES intensity around the surface contour at this photon energy.

II. EXPERIMENT

Experiments were performed at beam line ID08 at the European Synchrotron Radiation Facility (ESRF) in Grenoble, France. This beam line is capable of producing $\approx 10^{13}$ photons/s/0.1%BW on the sample and is equipped with a Scienta SES-2002 electron energy analyzer. Using this set-up it is possible to acquire ARPES spectra with an angular resolution of 0.15° along the slit and 0.2° in the perpendicular direction.

The Scienta analyzer was used in the angle mode; angular cuts were obtained parallel to the $\Gamma - (\pi, \pi)$ direction with a momentum resolution of 0.027 Å^{-1}. To obtain different angular cuts the sample was rotated in steps of 1.0° in relation to the analyzer, corresponding to a momentum resolution of 0.18 Å^{-1} perpendicular to the $\Gamma - (\pi, \pi)$ direction. Data presented here were recorded using an energy resolution of ≈ 100 meV for both the analyzer and the monochromator, giving a total resolution of $\Delta E \approx 140$ meV. Circularly polarized synchrotron radiation with an energy of 400 eV was used throughout the measurement.

The single crystal of $Nd_{1.85}Ce_{0.15}CuO_4$ was grown by the travelling solvent floating zone method [7, 8] and had a critical superconducting temperature of $T_c \approx 21K$. The sample was cleaved *in situ* and, using a liquid He cold finger, cooled down to a temperature of $\approx 24K$. During the measurement period temperature was monitored with a thermocouple placed inside the sample holder. LEED was used to check the surface quality and the orientation of the sample. The base pressure in the experimental chamber was below 5×10^{-11} mbar and no signs of sample degradation were seen during the 38-h measurement period. To obtain a reference for the Fermi level of the sample a gold foil was placed in electrical contact with it on the sample holder.

III. RESULTS AND DISCUSSION

In Figs. 1 and 2 we present $E - \vec{k}$ image plots of the ARPES spectral intensity along two different high-symmetry directions in the Brillouin zone. In the $\Gamma - (\pi, \pi)$ direction, Fig. 1, a dispersive feature which is present in all the cuprates, is seen. Dispersing towards the Fermi level it crosses it at $\vec{k_F} \approx (0.45\pi, 0.45\pi)$. This dispersion agrees with earlier measurements performed at lower photon energies [4, 5]. In the $(-\pi/2, -3\pi/2) - (\pi/2, -\pi/2)$ direction (parallel to the $\Gamma - (\pi, \pi)$ direction), see Fig. 2, two different dispersive features are crossing

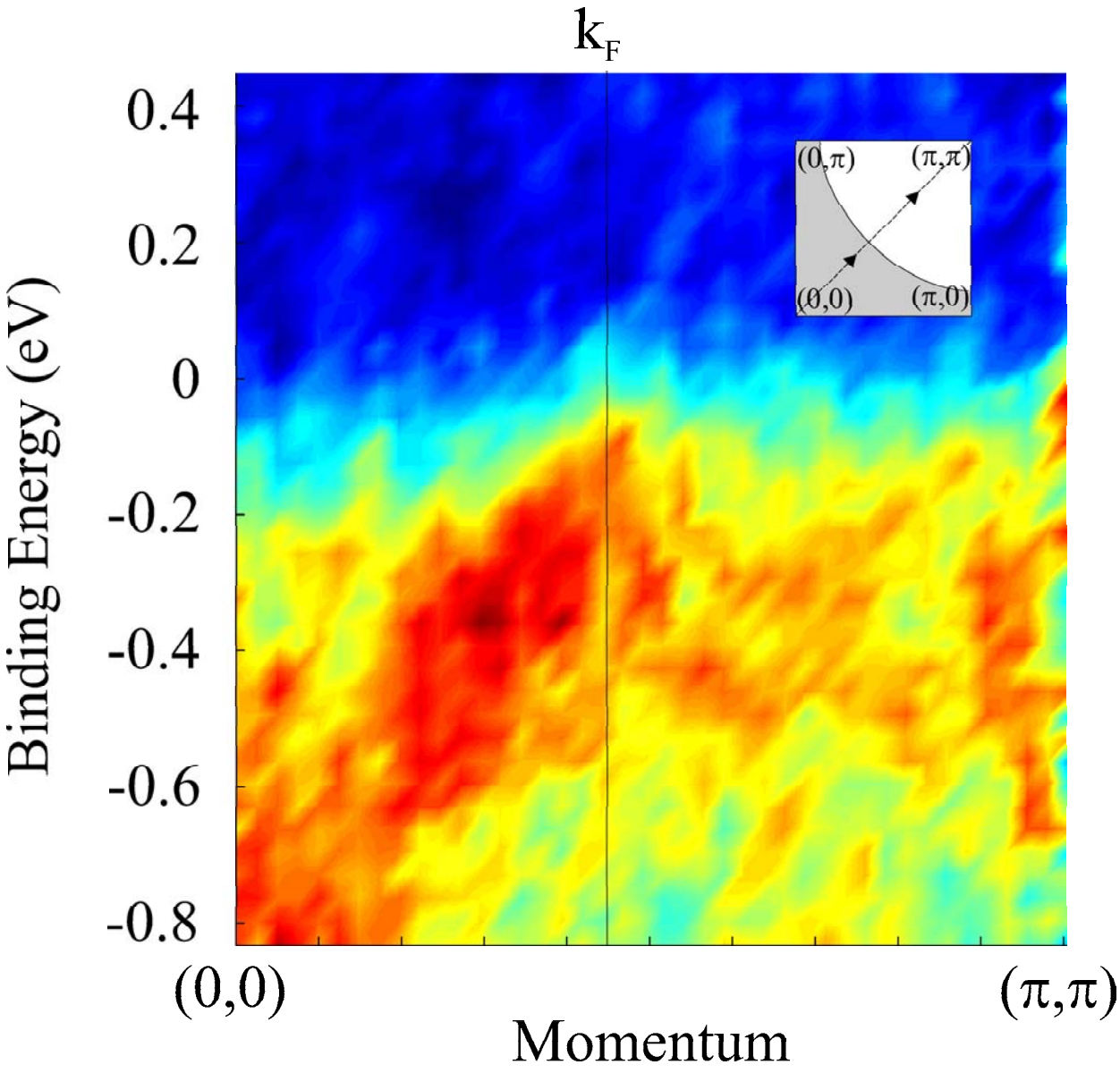

FIG. 1: ARPES spectral intensity at $h\nu = 400$ eV plotted as a function of binding energy and momentum for a cut in the $\Gamma-(\pi,\pi)$ direction, see schematic inset. A dispersive feature approaching E_F and crossing it at $|\vec{k_F}| \approx 45\%$ of the distance between Γ and (π,π) , is clearly seen.

the Fermi level at $|\vec{k_F}| \approx 36\%$ and $|\vec{k_F}| \approx 70\%$ of the distance between $(-\pi/2, -3\pi/2)$ and $(\pi/2, -\pi/2)$ respectively.

Besides the dispersive data in particular directions, we also have compiled a Fermi surface map by summing the ARPES intensity over a 136 meV energy window about the Fermi level, see Fig. 3. In agreement with data presented by Armitage *et al.* [4, 5] the Fermi surface is of the hole-type. To compensate for non-uniformities of the detector (analyzer) each ARPES

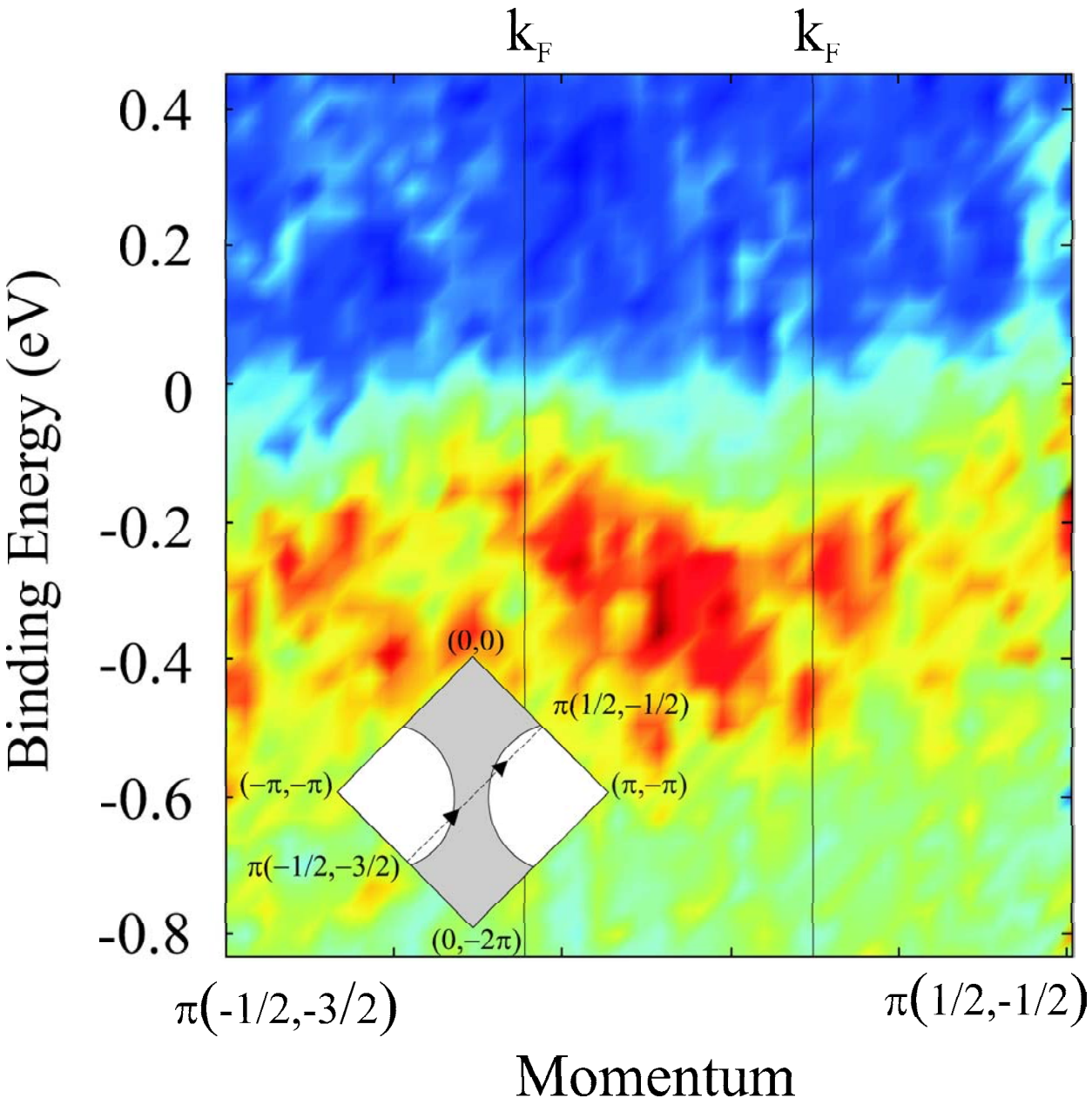

FIG. 2: ARPES intensity for a cut in the $(-\pi/2, -3\pi/2) - (\pi/2, -\pi/2)$ direction. Two dispersive features can be distinguished, one is crossing the Fermi level at $|\vec{k_F}| \approx 36\%$ and the other at $|\vec{k_F}| \approx 70\%$ of the distance between $(-\pi/2, -3\pi/2)$ and $(\pi/2, -\pi/2)$.

spectrum was normalised in the following way before the Fermi surface map was obtained. The data for each angle in an ARPES spectrum have been normalised to the integrated intensity (i.e. summing over all energies) for that particular angle.

In order to make a more detailed analysis of the Fermi surface shape we have added intensity contributions from k-points equivalent by symmetry over almost the entire map

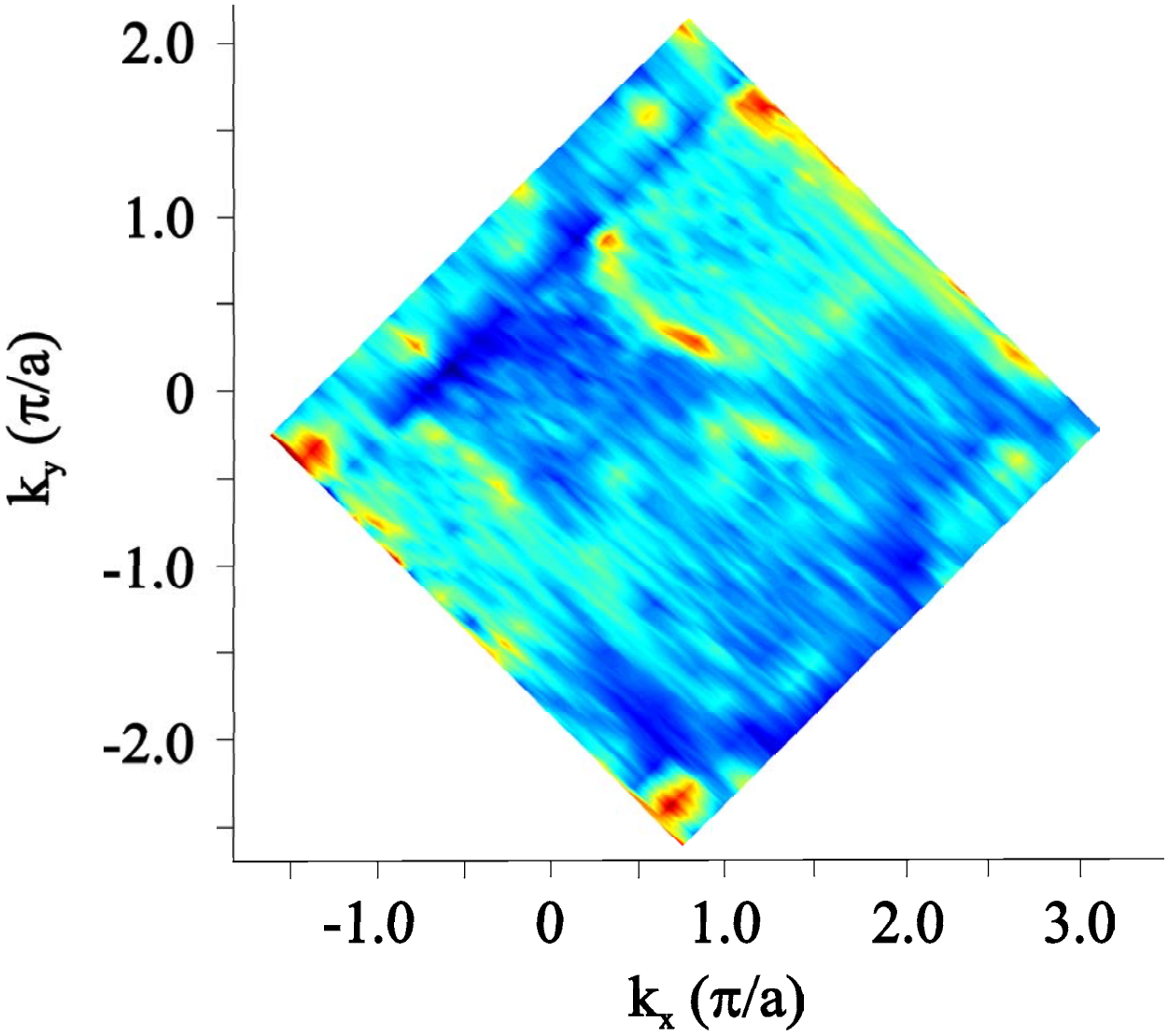

FIG. 3: Fermi surface plot obtained by energy integration of ARPES spectra over a 136 meV window (±68 meV) about the Fermi level. About 2.5 repetitions of the Fermi surface are seen.

displayed in Fig. 3. This results in a Brillouin zone octant, which in Fig. 4 has been duplicated eight times to reproduce the complete Fermi surface. The normalisation used to obtain this map is not the same as that used in Fig. 3. Here each ARPES spectrum has been normalised to the intensity integrated over the entire spectrum (i.e. summing over all energies and angles) before the integration about the Fermi level was done. This allows us to make more distinct conclusions from the distribution of intensity around the Fermi surface contour. It should also be pointed out that due to a non-uniform data sampling in k-space we had to apply some interpolation to our data when adding intensities from different k-points.

This kind of interpolation is however always implicit in making a continuous colorplot from a discrete dataset.

The Fermi surface of Fig. 4, compiled from the complete data set presented in Fig. 3, can be compared with the low energy data presented by Armitage *et al.* [4, 5]. As noted above the Fermi surface is of the hole-type. The volume is consistent with the value $1+x$ given by Luttinger's theorem [6]. With a measured filling level of 1.16 ± 0.05 the Luttinger theorem gives a doping level $x = 0.16$, which is in good accordance with our sample ($x = 0.15$). Hence, in spite of the increased bulk-sensitivity resulting from a high photon energy, we can confirm the volume (doping level) seen in low energy measurements. However, it is clear that our data deviates from that observed by these authors with regard to both the shape and the intensity distribution around the contour. Here it should be noted that we have used a wider energy window than Armitage *et al.* (136 meV instead of 30 and 60), which could to a limited degree influence the spectral characteristics.

The data of Armitage *et al.* [5] show an NCCO Fermi surface where spectral weight is suppressed in regions near $(0.65\pi,0.3\pi)$ and $(0.3\pi,0.65\pi)$ as compared to other parts of the surface contour. Although differences in the intensity distribution between the 16.5 and 55 eV data indicate that matrix-element effects are present, these authors, on the basis of a line-shape analysis, draw the conclusion that the observed effect is real and not only caused by matrix-element dependencies. The intensity distribution of Fig. 4 is however more uniform, showing no similarities with the modulations seen in the data of Armitage *et al.*

Armitage *et al.* [5] note that the regions where they measure suppressed intensity are located close to the intersections of the Fermi surface with the AF Brillouin zone boundary. Based on this and the fact that a line-shape analysis seems to indicate an increased scattering rate in the same regions, they argue that charge carriers there are subject to $\vec{Q} = (\pi, \pi)$ scattering. After a comparison with our data this interpretation seems more unlikely. In Fig. 4 there is no sign of the intensity modulations on the Fermi surface contour presented by the authors in Ref. 5. If there is a modulation in our Fermi surface data it is rather the opposite one to that displayed in Ref. 5 with increased intensity where they see suppressed and vice versa. The fact that we have used circularly polarized synchrotron radiation with $h\nu = 400$ eV, while Armitage *et al.* have used linearly polarized radiation with $h\nu = 16.5$ and 55 eV, suggests that matrix-element effects dependent on experimental geometry, photon energy and light polarisation might be important for the modulations seen in the low energy

data. The importance of matrix-element dependent effects [9] and photon energy dependence [10, 11] in ARPES measurements on the cuprates, especially BSCCO, has been demonstrated several times.

Previous ARPES measurements on $Nd_{2-x}Ce_xCuO_4$ ($x = 0.15$) performed at lower photon energies have shown a Fermi surface contour of rounded shape [4, 5] roughly in agreement with results from LDA calculations [12]; a qualitative skecth is given in Fig. 5. The Fermi surface of Fig. 4 however has a shape that deviates from these results. Here we see a shape with distinct but a bit rounded corners connected by nearly straight sections. With a photon energy of $h\nu = 400$ eV we are probing the electronic structure at larger depth as compared to the previous measurements by Armitage *et al.* performed at $h\nu = 16.5$ and 55 eV. By integrating along the surface contour we have verified having approximately the same doping level as these authors. This gives us reason to believe that the shape deviations we see could be caused by differences in the electronic structure between the outermost surface layer(s) and the deeper lying bulk structure. These structural differences can be related to several different phenomena.

A plausible explanation might be that in the topmost surface layers the effects of electronic correlations are suppressed as a result of the structural differences between the surface and the bulk layers. In that case it is not surprising to find a variation of the FS shape as a function of probing depth. The observed FS shape with pronounced corners and straight segments could hence be related to an increased influence from electronic correlations in the bulk region. A Fermi surface with straight segments has previously been observed in another of the copper oxide superconductors, namely LSCO. In that case the observation has been interpreted as an indication of 1D electronic behaviour. This suggests that our FS shape, much like a square with rounded corners, could to some degree be understood if 1D electronic character persists to a larger amount in the deeper lying bulk layers than in the surface region.

The doping evolution of the high-T_c cuprate Fermi surface can be described by the following scenarios. If the undoped insulating AF parent is viewed as a metal, a tight-binding model would give a square Fermi surface as qualitatively shown in Fig. 5 (a) [13]. Doping by introducing electrons to low doping levels gives a 'small' Fermi surface consisting of four small areas whose midpoints are the centres of the four Brillouin zone edges. The number of charge carriers (electrons) is given by the Fermi surface volume. With x being the number

of added electrons per formula unit the doped compound here has a Fermi surface volume proportional to x. With increased doping level there is a gradual transition to a 'large' Fermi surface (volume $\sim 1 + x$) centered around (π, π). In the case of NCCO the shape resulting from the latter scenario has been reproduced reasonably well by both LDA calculations [12], as schematically shown in Fig. 5 (b), and low energy ARPES measurements [4, 5].

A careful look at the 16.5 eV data of Armitage *et al.* reveals a flat area around the $(\pi/2, \pi/2)$ point. In our 400 eV data, Fig. 4, the flat region is larger and even more pronounced making the FS appear more or less like a square with somewhat rounded corners. The large degree of resemblance between Fig. 4 and Fig. 5 suggests that the electronic structure in the bulk region might be more influenced by that of the AF parent than it is in the surface layers.

In the above discussion concerning the variation of spectral intensity around the Fermi surface contour much attention was paid to the influence of matrix-element dependent effects. However, when the FS shape is discussed the situation is different since any matrix-element effects would not give drastic changes in the line-shape of acquired ARPES spectra. Hence the FS shape is in principle independent of any such effects.

In summary we have conducted angle resolved photoemission on a $Nd_{1.85}Ce_{0.15}CuO_4$ single crystal at a photon energy significantly higher than previously presented ($h\nu = 400$ eV). Our dataset, covering more than two repetitions of the Brilloiun zone, has been used to map out the Fermi surface. It is of the hole-type and has a volume in agreement with Luttinger's theorem ($\approx 1 + x$, where $x \approx 0.16$). In contrast to previous measurements at low energy we observe a Fermi surface of diamond like shape with almost straight sections. The increased bulk sensitivity suggests that this difference could be caused by a change in electronic structure between the outermost planes and the deeper lying ones. Furthermore, the observed distribution of spectral weight lends no support to the proposal of strong $\vec{Q} = (\pi, \pi)$ scattering in certain momentum space regions. In this case, the differences between our data and earlier low energy observations can most probably be attributed to matrix element effects.

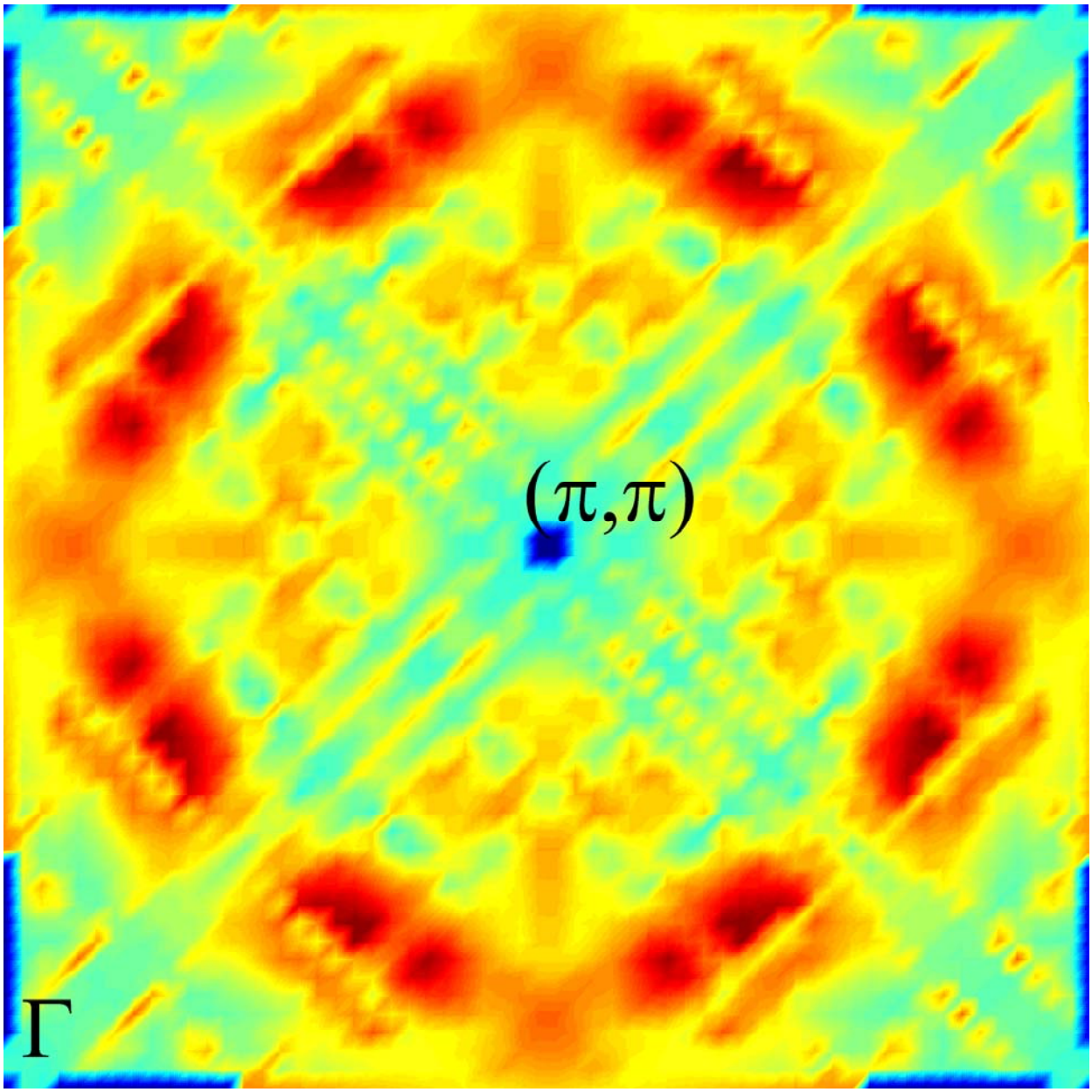

FIG. 4: Symmetrized Fermi surface plot obtained by adding intensities from symmetrically equivalent k-points over the complete Fermi surface map of Fig. 3. The resulting Brillouin zone octant is repeated eight times to get the shape of the complete Fermi surface.

Acknowledgments

Technical support from K. Larsson is gratefully acknowledged. This work was in part supported by the Swedish Research Council, the Swedish Foundation for Strategic research

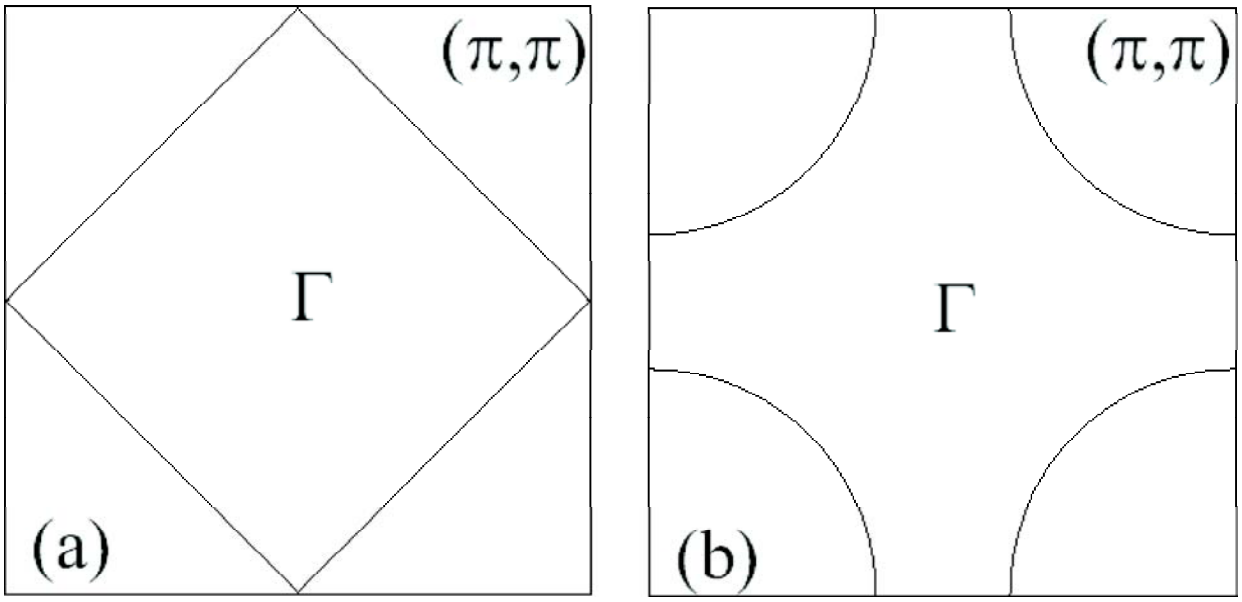

FIG. 5: Schematic shape of the high-T_c cuprate Fermi surface for two different cases. (a) The FS shape for the undoped AF parent compound as given by a tight-binding model. (b) The 'large' LDA-like FS obtained upon doping the parent compound to high doping levels.

and the Göran Gustafsson Foundation.

---

[1] N. P. Armitage *et al.*, Physica C **341**, 2083 (2000).

[2] A. Damascelli, Z. Hussain, and Z.-X. Shen, Rev. Mod. Phys. **75**, 473 (2003).

[3] N. P. Armitage *et al.*, Phys. Rev. Lett. **86**, 1126 (2001).

[4] N. P. Armitage *et al.*, Phys. Rev. Lett. **88**, 257001 (2002).

[5] N. P. Armitage *et al.*, Phys. Rev. Lett. **87**, 147003 (2001).

[6] J. M. Luttinger, Phys. Rev. **119**, 1960 (1960).

[7] V. H. M. Duijn, N. T. Hien, A. A. Menovsky, and J. J. M. Franse, Physica C **235-240**, 559 (1994).

[8] A. A. Nugroho, I. M. Sutjahja, M. O. Tjia, A. A. Menovsky, F. R. de Boer, and J. J. M. Franse, Phys. Rev. B **60**, 15379 (1999).

[9] A. Bansil and M. Lindroos, Phys. Rev. Lett. **83**, 5154 (1999).

[10] P. V. Bodganov *et al.*, Phys. Rev. B **64**, 180505 (2001).

[11] Y. D. Chuang *et al.*, Phys. Rev. Lett. **83**, 3717 (1999).

[12] S. Massidda, S.Hamada, J. Yu, and A. J. Freeman, Physica C **157**, 571 (1989).

[13] D. W. Lynch and C. G. Olson, *Photoemission Studies of High-Temperature Superconductors* (Cambridge University Press, Cambridge, 1999).